ACS APPLIED ENERGY MATERIALS

www.acsaem.org Article

Surface-Plasma-Induced One-Pot Synthesis of N,S-Carbon Dot Intercalated MoS_2/Graphene Nanosheets for Highly Efficient Hydrogen Evolution Reaction

Van Dien Dang, Chang-Yu Hsiao, Phuoc Anh Le, Van Qui Le, Dang Ho Phuong Thao, Thi-Hien Do, and Kung-Hwa Wei*

Cite This: *ACS Appl. Energy Mater.* 2022, 5, 12817−12827 Read Online

ACCESS | Metrics & More | Article Recommendations | Supporting Information

ABSTRACT: Herein, a facile and rapid surface-plasma-induced method was adopted for the one-pot synthesis of a 2D/0D/2D hybrid nanostructure consisting of N,S co-doped carbon dots (NSCD) intercalated few-layer MoS_2/graphene nanosheets (MoS_2/G) as an excellent catalyst for the hydrogen evolution reaction (HER). In this process, bulk MoS_2 and graphite foil served as the sources of MoS_2 and graphene nanosheets, respectively, while glucose and thiourea served as the source of NSCD. The sturdy integration of 0D NSCD and 2D MoS_2/G in a well-constructed ternary composite provided a huge number of edge active sites with tunable and extraordinary physicochemical properties for electron transport, facilitating HER performance. The optimal NSCD@MoS_2/G exhibited a superior catalytic activity toward HER with a low onset potential (37 mV), an overpotential of 98 mV at 10 mA cm^{-2}, and a Tafel slope as small as 53 mV dec^{-1}, which were better than other 2D electrocatalysts. The increase in double-layer capacitance for NSCD@MoS_2/G (12.2 mF cm^{-2}), which was 2-fold of the MoS_2/G sample, is strong evidence of the large catalytic edge sites and electrical coupling in the NSCD@MoS_2/G ternary system. Moreover, the strong bonding and interaction between NSCD and MoS_2/G nanosheets enabled outstanding long-term stability and structural integrity, displaying 95 and 90% activity retention at 10 and 50 mA cm^{-2} after 48 h i−t test, respectively. This approach paves the way to efficient syntheses of 2D/0D/2D heterostructures with great potential for various energy-related applications.

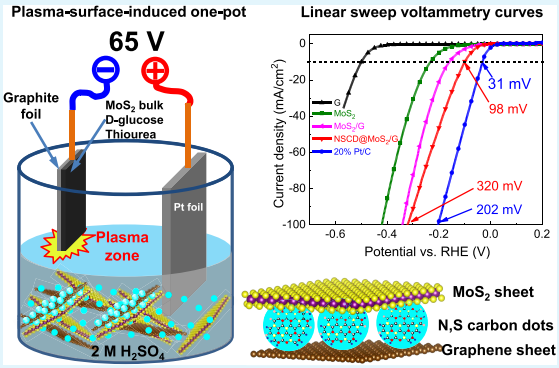

KEYWORDS: *electrochemical-induced plasma, carbon dots, MoS_2 nanosheets, graphene nanosheets, hydrogen evolution reaction*

■ INTRODUCTION

Concerns about environmental pollution and possible energy crises associated with fossil fuel exploitation have motivated considerable efforts to develop clean energy sources. Producing hydrogen (H_2), a promising energy carrier, through water splitting appears to be an extremely sustainable strategy for achieving clean energy. Although Pt- and noble metal-based materials have been used as the most effective HER electrocatalysts, the scarcity and high cost limit their large-scale applications. Therefore, earth-abundant and cost-effective materials are being sought to construct highly active HER catalysts.

Two-dimensional transition metal dichalcogenides (TMD) have attracted considerable attention for electrocatalytic HER applications because of their abundance, large active sites, and advanced electrochemical properties after certain surface modifications.[1,2] For example, HER activity through the electrochemical reactions of layered Mo-based catalysts (MoS_2, $MoSe_2$, MoP, and Mo_2C) has been reported in both acidic and basic media.[3−8] Among these electrocatalysts, layered MoS_2 has received the most attention because the exposed active S atoms on its edges can form strong bonds with H^+ in the electrolyte solution, which is beneficial for initiating HER activity.[9] However, the relatively low conductivity of MoS_2 limits its catalytic performance. Accordingly, many attempts have been made to improve the catalytic HER activity of layered MoS_2 by enhancing the number of its active sites, even creating some defects in the basal plane and boosting the degrees of charge transfer between them.[10−13] Coupling with other heteroatoms has been considered an effective strategy for improving the electrical conductivity and catalytic HER performance of MoS_2 through enhanced electronic interactions and the formation of reactive interfaces.

Received: July 29, 2022
Accepted: September 27, 2022
Published: October 7, 2022

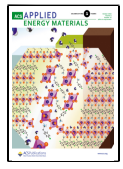

Downloaded via NATL YANG MING CHIAO TUNG UNIV on November 7, 2023 at 07:26:44 (UTC).
See https://pubs.acs.org/sharingguidelines for options on how to legitimately share published articles.

ACS Publications © 2022 American Chemical Society

https://doi.org/10.1021/acsaem.2c02401
ACS Appl. Energy Mater. 2022, 5, 12817−12827

Scheme 1. (a) Design and (b) Experimental Setup; (c) Structure Illustration of NSCD@MoS_2/G Composite through the One-Pot Plasma Process

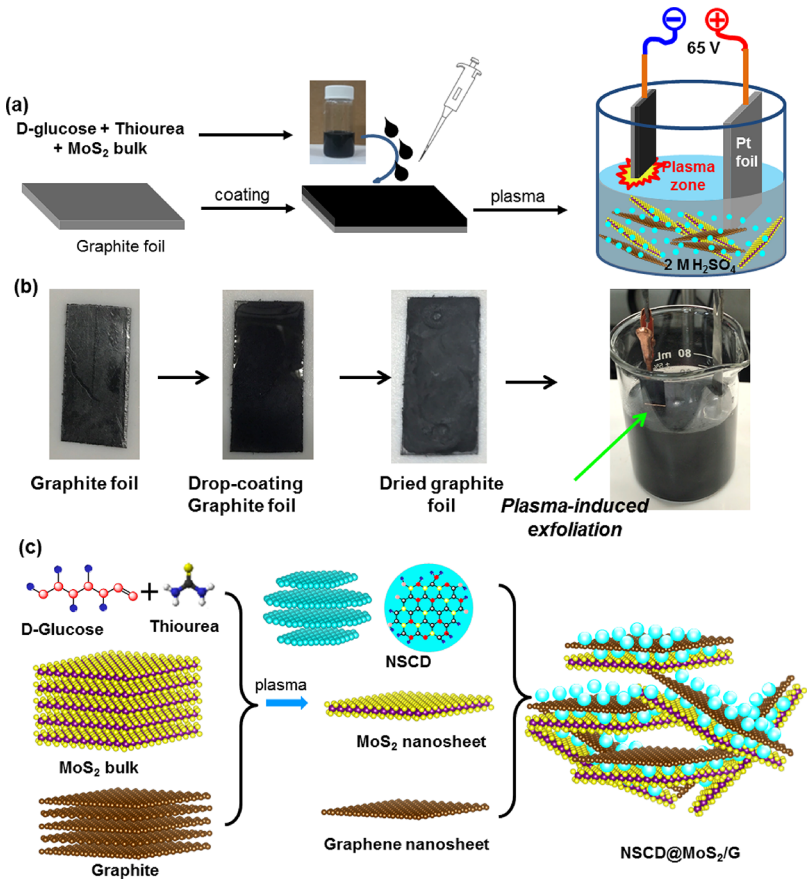

Graphene nanosheets (G) are promising co-catalysts because of their high specific surface area, excellent conductivity, good stability, and a few-layer configuration.[14] It was expected that employing G as a loading matrix would enhance the conductivity of the system and thus improve the activity of embedded electrocatalysts.[15] Based on the different features of these component materials, the combination of MoS_2 and G would be a promising approach to enhancing the conductivity and durability of materials for application in the HER. However, the catalytic performance of MoS_2/G binary composites remains far from satisfactory compared to that of Pt-based systems.[16] Also, their catalytic stability is readily attenuated after long electrochemical processes, owing to the agglomeration and/or oxidation of metal-based components. Hence, it is necessary to enhance the local electronic and geometric structures by combining them with another material, which is considered a means to improve the catalytic efficiency and stability of such binary composite.

Carbon nanodots (CD), as a new type of 0D carbon nanomaterial, have been incorporated into various semiconductors for H_2 production because of their superior electrochemical activity and flexibility in both acidic and basic electrolytes.[17,18] The CD possesses an abundance of functional groups, which can incorporate with metal ions to form a stable composite.[19] Moreover, the carbon structure can support and promote electrical conductivity during the HER process owing to its sp^2-/sp^3-hybrid carbon core and easy-to-functionalize electronic properties.[20] It has been documented that heteroatom doping/modification of CD can promote electron transfer by tuning their electron density and the intrinsic properties of composites, resulting in higher HER activity.[21−23] Therefore, we expected that incorporating nitrogen-and-sulfur-co-doped carbon nanodots (NSCD) into a MoS_2/G composite would be a promising strategy for improving the electrochemical properties (e.g., increasing the number of edge sites and the stability), thereby enhancing the catalytic HER performance.

The catalytic activity of any composite is highly dependent on its surface structure, which is associated with the synthetic technique. The conventional methods, including hydrothermal processing, chemical vapor deposition, and chemical exfoliation, have been commonly used for synthesizing MoS_2/G nanosheets and carbon dots. However, they all require many time-consuming steps and costly special equipment.[24,25] Therefore, the quest remains to find rapid, facile, and inexpensive methods to synthesize materials for efficient HERs, with the ultimate goal of realizing H_2 energy. Fortunately, electrochemical exfoliation has been reported as a rapid method for the direct mass-production of two-dimensional materials with few layers through the exfoliation of bulk materials.[4,26]

To the best of our knowledge, surface-induced plasma processes have never been used to produce NSCD@MoS_2/G ternary composites as electrocatalysts for the HER, particularly in a one-pot process. In this study, we employed *in situ* surface-plasma-induced electrochemical reactions as a rapid, facile, and cost-effective method for preparing an NSCD@MoS_2/G composite for the HER. Incorporating the as-prepared

https://doi.org/10.1021/acsaem.2c02401
ACS Appl. Energy Mater. 2022, 5, 12817−12827

NSCD with a diameter of approximately 5 nm into MoS_2/G (200−300 nm) could tune the composite structure and increase the number of active sites, lowering overpotential as well as superior durability. Thus, such ternary composites produced by plasma-induced processes appear to be promising materials for large-scale HER activity.

■ EXPERIMENTAL SECTION

Preparation of Composite Film as a Cathode for Plasma Process. MoS_2 powder (31 mg), D-glucose (1.5 mg), thiourea (1.5 mg), and PVDF (3 mg) were dispersed in NMP (1 mL) under vigorous stirring for 30 min to obtain a homogeneous slurry. As shown in Scheme 1a,b, the as-prepared slurry was coated dropwise on a graphite paper (1 × 2 cm^2, 27 mg) and laid on a hot plate (60 °C) until the slurry dried completely and formed a bilayer film and then kept in an oven at 80 °C for 1 h. For comparison, graphite paper alone (G), MoS_2/G composite with different weight ratios (Table S1), and MoS_2 film alone (drop-coated on Mo foil instead of graphite paper) were conducted with the same procedure. In addition, different weight ratios of D-glucose and thiourea were prepared to assess the effect of NSCD on the catalytic activity (Table S2). For comparison, pure carbon dot-anchored MoS_2/G (CD@MoS_2/G) was synthesized with the same procedure except for the absence of thiourea.

Preparation of NSCD@MoS_2/G Composites. The NSCD@MoS_2/G composites were prepared by electrochemical plasma in a 50 mL 2 M H_2SO_4 electrolyte (Scheme 1). A Pt foil (3 × 6 cm^2) immersed 2 cm into the electrolyte was used as an anode, while the as-prepared film was used as a cathode. The two electrodes were connected to a DC power supply (Lin VAC TECH, Taiwan). Under an applied voltage of 65 V, the cathode was moved down slowly to touch the electrolyte surface to induce the plasma. The plasma jets exfoliated the bulk MoS_2 into MoS_2 nanosheets, graphite to graphene, and D-glucose and thiourea to N,S do-coped carbon dots (NSCD). After 45 min of cathodic plasma induction, the exfoliated composite was subjected to tip ultrasonication (50 W) for 1 h. The supernatant was collected by centrifugation (1500 rpm, 5 min), and the non-exfoliated solid was removed. The obtained solution was washed sequentially with 1% NaOH, deionized water, and ethanol by centrifugation (9000 rpm, 15 min), dried at 80 °C for 4 h, and then stored in a tube for further use. The NSCD was synthesized with the same procedure except for replacing graphite paper by a Mo rod and dissolving NSCD precursors in an electrolyte for the plasma reaction. The obtained yellowish solution was then dialyzed for 8 h and freeze-dried to collect solid NSCD. The video illustrating the plasma process is attached in the Supporting Information.

Materials Characterization. The morphology of the as-prepared composite was characterized by SEM (Hitachi SU8000) and TEM (JEOL F200). The structure and chemical state of NSCD@MoS_2/G-based materials were characterized by AFM (Agilent 5500), XRD (D2 Bruker), Raman (Jobin Yvon, Horiba), BET (ASAP 2020), and XPS (Escalab 250Xi, Thermo Scientific). An elemental analyzer (elementar vario EL cube) was used to simultaneously determine C, H, N, S, and O in samples.

Electrochemical Measurements. The catalyst slurry was prepared by dispersing 3 mg of NCD@MoS_2/G in 1 mL of DMF under 30 min of sonication. Subsequently, 6 μL of the slurry was dropped slowly on a glassy carbon electrode (GCE, a diameter of 3 mm, 0.257 mg cm^{-2}) and dried at 45 °C for 1 h. Afterward, the catalyst-coated GCE was covered by 3 μL of Nafion (5 wt %) and dried at room temperature for 1 h. The NSCD@MoS_2/G-coated GCE, Ag/AgCl (3 M NaCl) electrode, and graphite rod were used as working, reference, and counter electrodes in 0.5 M H_2SO_4 electrolyte, respectively. Cyclic voltammetry (CV) and LSV (scan rate of 5 mV/s) were examined within the potential range from −0.57 to 0.23 V vs RHE using a three-electrode system (CHI 611B electrochemical workstation). The LSV curves were recorded after 20 cycles of stable CV curves. EIS was performed in the range of 0.1−10^5 Hz and an amplitude of 5 mV using a three-electrode electrochemical workstation (Zahner Zenium Z 2.23). The long-term durability test was performed using the chronopotentiometry method at a constant current density of 10 and 50 mA cm^{-2}. The double-layer capacitance (C_{dl}) was determined from the linearity slope of the plot of scan rates against the difference between anodic and cathodic current densities at the same potential of CV in the double-layer region (Δj). In all measurements, the current densities were calculated based on the geometric surface area of the GCE (0.07 cm^2), while the potential versus RHE (V_{RHE}) was converted from measured potentials (for Ag/AgCl electrode) as $E_{RHE} = E_{Ag/AgCl} + E_{Ag/AgCl\ vs\ NHE} + 0.059$ pH ($E_{Ag/AgCl\ vs\ NHE}$ = 0.209 at 25 °C). Gas chromatography (Agilent 7890 with thermal conductivity detector) was used to detect the H_2 produced from the HER activity by the NSCD@MoS_2/G electrode.

■ RESULTS AND DISCUSSION

Scheme 1a illustrates the one-pot synthetic procedure we used to prepare the NSCD@MoS_2/G ternary composite through one-pot surface-plasma-induced exfoliation of bulk MoS_2 to MoS_2 nanosheets, graphite to graphene nanosheets, and coupling reaction of D-glucose and thiourea to NSCD. The setup for the electrochemical induced surface plasma process is described in detail in the Experimental Section, and the experimental photos are shown in Scheme 1b. Tables S1 and S2 present the various weight ratios of the precursors used for synthesizing the MoS_2/G and NSCD@MoS_2/G composites, respectively. We performed the induced-plasma process under low temperature (electrolyte was maintained at 60 °C) in ambient conditions within a short period of time (45 min).

D-Glucose, thiourea (the precursors of the NSCD), and bulk MoS_2 (the precursor of the MoS_2 nanosheets) were mixed well in a slurry state and deposited on a thin graphite foil substrate to form a bilayer film that served as the cathode in the electrochemical process. Pt foil immersed 2 cm into the 2 M H_2SO_4 electrolyte served as the anode. The induced-surface-plasma occurred by asymmetric electric field strength, owing to the large difference in the contact areas between the cathode (contacted with electrolyte on the surface) and anode (immersed in the electrolyte) in the electrochemical reaction. Accordingly, under an applied voltage of 65 V, the surface of the cathode that was contacted with electrolyte appeared plasmic and thus experienced an extremely high temperature (between 2000 and 3000 K), while the remaining part of the cathode remained in room temperature, therefore generating a large temperature gradient.

Because of the different degrees of resultant thermal expansion between the cathode and its solid−liquid interface with the electrolyte (under the high-temperature plasma), an in-plane shear force was generated and frustrated the van der Waals forces between the in-plane layers of bulk MoS_2 and graphite. Therefore, the bilayer film was exfoliated to form MoS_2 nanosheets and G nanosheets, and NSCD formed through the reaction of D-glucose and thiourea and intercalated between the layers of MoS_2 and G. As shown in Scheme S1, under plasma process, C═C, N−C, and S−C bonds were constructed from the precursors for the basic structure of N,S-co-doped carbon dots, while water molecules were formed by the interaction of hydrogen atoms and hydroxyl groups on glucose; simultaneously, amide could be formed between $-NH_2$ and −COOH with the presence of amine in the reaction and pyrrolic N could be built by intramolecular dehydrolysis between amide and COOH groups. As a result, the NSCD was mixed well with the exfoliated MoS_2 and G nanosheets to form a homogeneous NSCD@MoS_2/G ternary composite. The lower intensity of the signal at the 2θ value of 14° in the XRD spectrum, and broader full widths at half-

https://doi.org/10.1021/acsaem.2c02401
ACS Appl. Energy Mater. 2022, 5, 12817−12827

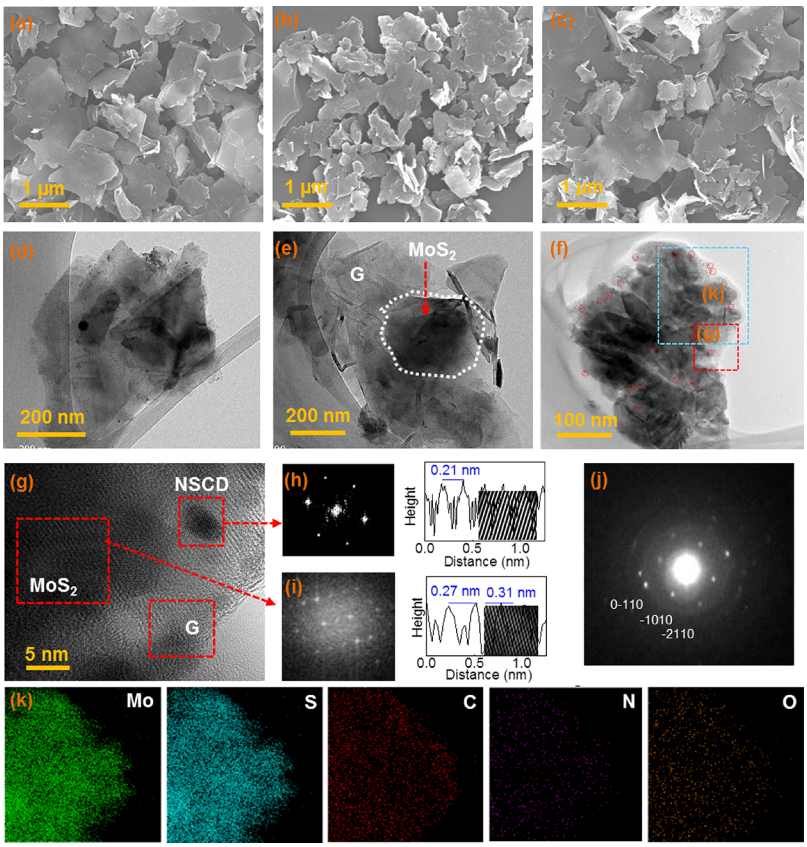

Figure 1. (a–c) SEM images of the (a) MoS_2, (b) MoS_2/G, and (c) NSCD@MoS_2/G samples; (d–f) TEM images of the (d) MoS_2, (e) MoS_2/G, and (f) NSCD@MoS_2/G samples; (g) HRTEM image of the NSCD@MoS_2/G composite; (h, i) FFT images and interplanar spacings with inversed FFT of (h) the NSCD and (i) MoS_2; (j) SAED pattern of the NSCD@MoS_2/G composite; (k) EDS mapping of NSCD@MoS_2/G.

maximum (FWHMs) of the peaks in the Raman spectrum of MoS_2, provided evidence for the increase in the MoS_2 interlayer distance after doping with NSCD. The formation of such a ternary composite structure is one of the key factors toward improving the HER performance. Scheme 1b displays a schematic representation of the structure of the composite. We expected this synthesis strategy to result in an excellent HER composite catalyst.

We used scanning electron microscopy (SEM) and transmission electron microscopy (TEM) to observe the morphologies and sizes of the components in the NSCD@MoS_2/G composites. Figure 1a exhibits that the MoS_2 nanosheets formed after the induced-plasma process had a lateral size of 300 nm. Figure 1b reveals smaller MoS_2 nanosheets in the MoS_2/G composite, confirming their successful exfoliation.

Figure 1c shows that the thin G nanosheets were scattered around randomly distributed MoS_2 nanosheets and NSCD. The as-prepared MoS_2 appeared almost transparent in the TEM image in Figure 1d, confirming its ultrathin nanosheet morphology. Figure 1e exhibits the TEM image of the MoS_2/G binary composite, indicating that the layered MoS_2 nanosheets were supported on the G surface. Figure 1f presents a high-resolution transmission electron microscopy (HRTEM) image of the ternary composite, with the TEM image of the localized square marked in Figure 1g, indicating the presence of the three components (NSCD and MoS_2 nanosheets deposited on G nanosheets). Figure 1h reveals the hexagonal lattice structure of the NSCD, with a lattice spacing of 0.21 nm derived from the HRTEM image, corresponding to the *d*-spacing of the (1−100) plane. Figure 1i displays lattice spacings of 0.27 and 0.31 nm corresponding to the (001) and (002) planes of MoS_2, respectively.[27,28] In comparison, Figure 1j shows that the SAED pattern of the NSCD@MoS_2/G composite indicates the coexistence of few-layer G sheets and rings associated with the (111) and (200) planes of graphitic carbon in the NSCD.

Figure S1 presents SEM, TEM, and fast Fourier transform (FFT) images and the interplanar spacing of the G material. The lattice spacing of 0.24 nm confirms the sp^2-hybrid carbon network of G.[29] Furthermore, the field-emission scanning transmission electron microscopy (FE-STEM) elemental mapping of the NSCD@MoS_2/G composite in Figure 1k reveals that the NSCD was deposited firmly on the surface of the MoS_2/G composite, in which all of the elements (Mo, S, C, N, and O) were uniformly distributed.

Figure 2a displays the atomic force microscopy (AFM) image of 5%-NSCD@MoS_2/G, indicating the step height of NSCD@MoS_2/G. We observed that the step height of composite varied in the wide range. The height of 1 nm could be typical of NSCD, while the height in the range of 5.8−49 nm could probably present for MoS_2 and G.[30,4] This result confirmed the coexistence of three components of the as-prepared NSCD@MoS_2/G, which comprises a few-layer to multiple-layer nanosheets with intercalated carbon dots after the one-pot cathodic plasma exfoliation process.[31]

We used X-ray diffraction (XRD) to determine the phases of the composites; Figure S2 displays the typical peaks found in the XRD patterns of graphite, bulk MoS_2, and the NSCD. Figure 2b signifies the presence of crystal structures of 2H- and

https://doi.org/10.1021/acsaem.2c02401
ACS Appl. Energy Mater. 2022, 5, 12817−12827

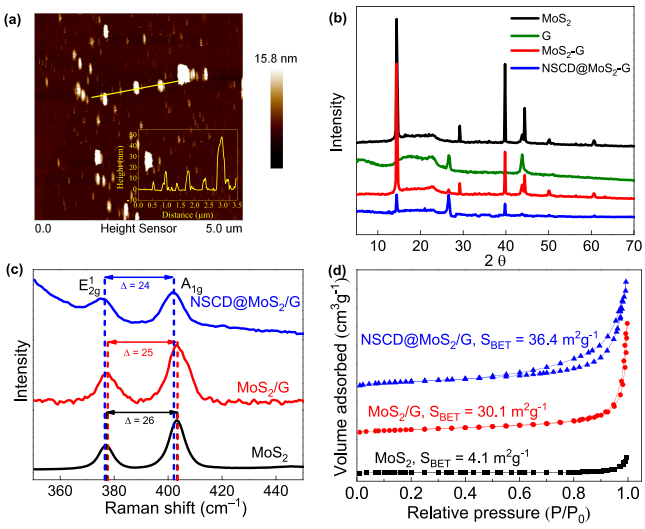

Figure 2. (a) AFM image of 5%-NSCD@MoS2/G; (b) XRD patterns, (c) Raman spectra, and (d) BET surface area of NSCD@MoS2/G-based composites.

1T-MoS_2, with a symmetry difference between the trigonal prismatic-coordinated 2H-MoS_2 and the distorted octahedral-coordinated 1T-MoS_2 (JCPDS #37-1492).[6,7,32] The intensity of the (002) peak at 2θ of 14.5°, provided by bulk MoS_2, was lower in the pattern of the NSCD@MoS_2/G-based composites, confirming the successful formation of MoS_2 nanosheets.[33] Thus, doping of the NSCD restacked the MoS_2 and G layers. Moreover, the peak at a 2θ value of 12.7° represents the NSCD in the NSCD@MoS_2/G composite. The peaks at 2θ values of 29.3 and 44.4° were not found in the pattern of the NSCD@MoS_2/G composite, which was attributed to the stacking of the conjugated Mo−S bonds and formation of interlayers of the composite in the presence of NSCD.

We used Raman spectroscopy to characterize the vibrations resulting from the different structures in the various composites. Figure 2c presents the Raman spectra of MoS_2, MoS_2/G, and NSCD@MoS_2/G, with typical peaks appearing at 377 and 403 cm^{-1}, corresponding to the E_{2g}^1 (in-plane, opposite vibration of two S atoms concerning the Mo atom) and A_{1g} (out-of-plane, vibration of only S atoms in the opposite direction) signals of MoS_2 nanosheets, respectively. This result indicates that the conductive metallic 1T and semiconducting 2H phases of MoS_2 nanosheets coexisted in these samples.[34,35] The FWHMs of the A_{1g} (out-plane) and E_{2g}^1 (in-plane) peaks of the NSCD@MoS_2/G composite (10.1 and 9.4 cm^{-1}, respectively) were broader than those of the MoS_2/G composite (8.0 and 7.8 cm^{-1}, respectively) and pristine MoS_2 nanosheets (7.2 and 6.6 cm^{-1}, respectively). This difference suggests that doping of the NSCD induced phonon confinement in the ultrathin nanosheets and induced some defects in the MoS_2 structures, potentially enhancing HER activity.[33] Furthermore, the shifts of −1 and − 2cm^{-1} of the A_{1g} modes of MoS_2/G and NSCD@MoS_2/G, respectively, suggest weaker interlayer van der Waals forces caused by additional interactions of the widened interlayer spacing of MoS_2.[30,36] Figure S3a features characteristic bands at 1344,

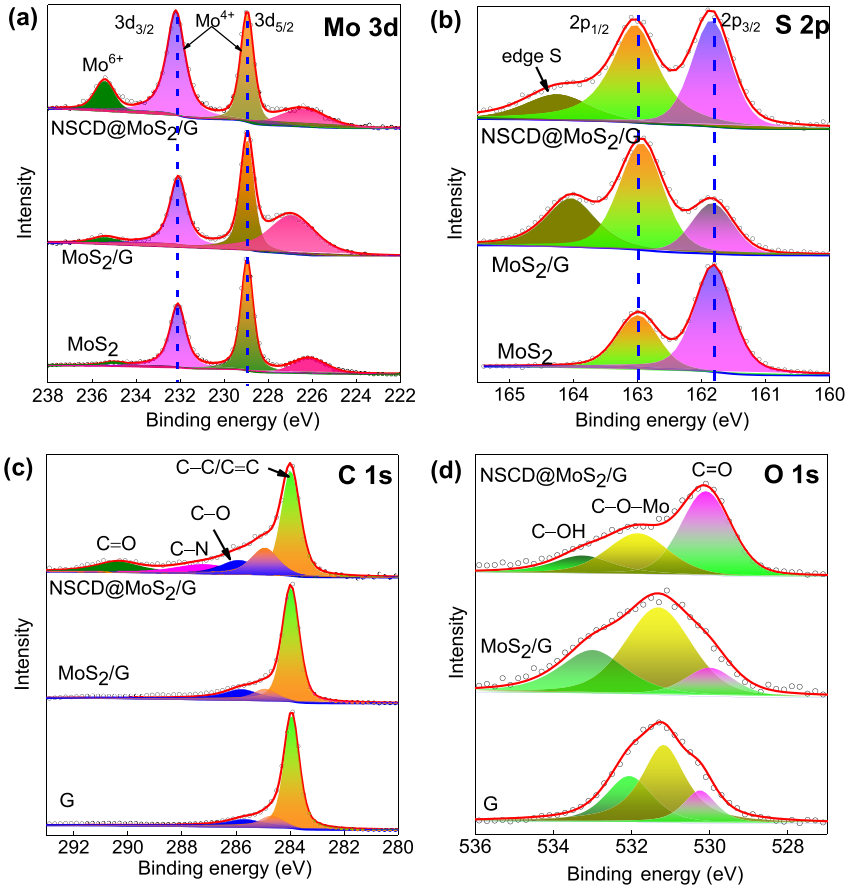

Figure 3. Deconvolution of XPS peaks: (a) Mo 3d, (b) S 2p, (c) C 1s, and (d) O 1s of NSCD@MoS_2/G.

https://doi.org/10.1021/acsaem.2c02401
ACS Appl. Energy Mater. 2022, 5, 12817−12827

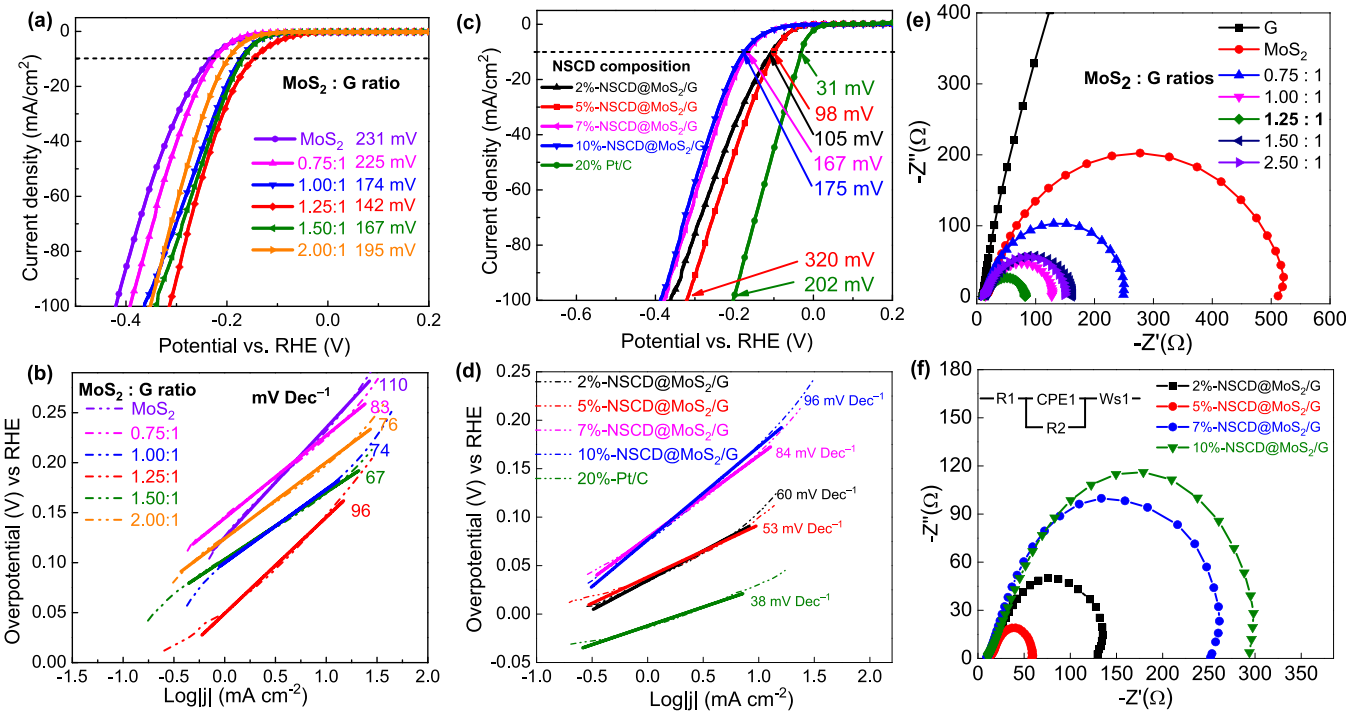

Figure 4. (a, b) Current densities and corresponded Tafel curves of MoS_2/G binary composite at different weight ratios, respectively; (c, d) current densities and corresponded Tafel curves of NSCD@MoS_2/G at different amounts of NSCD, respectively; (e, f) Nyquist plots of the MoS_2/G binary composite at different weight ratios and NSCD@MoS_2/G ternary composite at different amounts of NSCD, respectively.

1573, and 2689 cm^{-1}, representing the D (defects and layer disorder), G (E_{2g} phonon), and 2D (second-order vibration of D band) signals of G, respectively.[37] The 2D/G ratio, which is related to the degree of recovery of sp^2-hybridized C═C bonds (graphitization) in graphitic structures, implied the presence of high-quality few-layered G in the NSCD@MoS_2/G composite.[24] Figure S3b confirms the existence of edge disorder in the sp^2- and sp^3-hybridized carbon atoms and the surface defect states of the NSCD. The I_D/I_G ratio of 0.94, which is close to unity for a defected material, indicates that the exfoliation of D-glucose during the plasma process led to growing disorder and an amorphous carbon structure within the NSCD.[38]

We also measured the BET specific surface area of the samples to provide more details of the active sites. Figure 2d illustrates the typical type IV nitrogen adsorption/desorption isotherms with H3 hysteresis loops with P/P_o values ranging from 0.5 to 1, demonstrating the coexistence of meso- and macropores, while the P/P_o value lower than 0.5 indicates the existence of micropores. The pore size distribution (Figure S4, SI) shows model curves with peaks at 22, 50, and 70 nm, depicting the existence of the meso-macroporous structure of NSCD@MoS_2/G.[39] Moreover, the higher BET surface area (S_{BET}) for the NSCD@MoS_2/G ternary composite, as compared to that of MoS_2/G binary composite, confirms that the incorporation of NSCD increased the surface area and thus possibly the active sites, being consistent with the Raman result.

We used X-ray photoelectron spectroscopy (XPS) to determine the chemical binding states and quantitative chemical compositions of the NSCD@MoS_2/G-based composites. Figure S5a presents the XPS survey spectra of the materials, including the elements Mo, S, C, O, and N and their corresponding binding energies. The presence of monolayer MoS_2 could be determined from the Mo 3d and S 2p binding energies. Figure 3a illustrates the peaks at 232.2 and 229.0 eV, characteristics of the Mo $3d_{3/2}$ and $3d_{5/2}$ binding energies of Mo^{4+}, respectively,[40] in the three samples; they are the predominant oxidation states of the 1T phase.[41,42] It is noteworthy that the traces of Mo^{6+} species, resulting from the oxidation of Mo^{4+}, were not detected in the MoS_2 sample; it can be found at 235.5 eV in the spectra of the MoS_2/G and NSCD@MoS_2/G composites.[43] Therefore, we can state that the addition of the G nanosheets and NSCD resulted in these peaks shifting to lower binding energies, suggesting partial charge transfer among the MoS_2, G nanosheets, and NSCD.

Figure 3b displays the high-resolution S 2p XPS spectra of the MoS_2 and MoS_2/G samples; two peaks, for S $2p_{1/2}$ and $2p_{3/2}$ binding energies, appeared at 162.9 and 161.8 eV, respectively, indicating that the dominant oxidation state was S^{2-} in the 1T phase.[34,44] Moreover, a peak at 164 eV in the spectra of the MoS_2/G and NSCD@MoS_2/G composites indicates the presence of single-valent sulfide ions (S_2^{2-}), possibly bridging S_2^{2-} or apical S_2^{2-} species.[45] In addition, all of the peak positions for the NSCD@MoS_2/G composite were blue-shifted relative to those for the MoS_2/G and pure MoS_2 samples, implying that the presence of the NSCD triggered the formation of exfoliated metallic 1T (1T-MoS_2) phases, prior to 2H phases. Note that the 1T-MoS_2 phase can facilitate electron transport, potentially enhancing catalytic performance relative to the semiconducting 2H phase.[46] Hence, electrons may be transferred from NSCD to MoS_2/G nanosheets, leading to the interatomic charge polarization in NSCD to the MoS_2/G composite, which could facilitate the HER activity.

Figure 3c shows that the C 1s peaks for G had two components: for C—C/C═C species at 284.0 eV and for C—C/C—H species at 285.6 eV.[47] We assign the new peaks appearing in the spectrum of the NSCD@MoS_2/G composite

https://doi.org/10.1021/acsaem.2c02401
ACS Appl. Energy Mater. 2022, 5, 12817−12827

at binding energies of 290.4 and 287.5 eV to C═O and C−O bonds, respectively. The peak at 286.0 eV assigned to C−N/C−O coordination confirms the doping of heteroatoms (N atoms) from thiourea of NSCD.[48] Figure 3d proclaims the presence of peaks in the O 1s spectrum at 533.2, 531.8, and 530.1 eV, characteristic of C−OH, C═O, and C−O bonds, respectively.[49] The blue-shift of the G peak at 531.1 eV after adding Mo (531.3 eV) and the NSCD (531.8 eV) implies the establishment of C−O−Mo bonds, which are usually located in the range of 530−533 eV.[50] Figure S5b displays two peaks at 394.7 and 398.5 eV in the N 1s spectra, which are representatives of C−N bonds and pyridinic N atoms.[51] This result confirms the incorporation of N atoms into the NSCD, and G would contribute significantly to enhancing the surface electrolyte wettability and catalytic HER performance of the NSCD@MoS_2/G electrode. Overall, the XPS results illustrate the combination of C-, N-, and S-containing precursors (D-glucose and thiourea) under a heating condition to form NSCD, which was then compounded with MoS_2/G nanosheets that were generated from surface plasma. The coupling interface of MoS_2/G nanosheets modified with NSCD was effectively optimized to form the NSCD@MoS_2/G composite as an integrated architecture, which could further improve the electron transfer for efficiently catalytic activity and stability. Furthermore, elemental analysis was carried out to confirm the existence of C, H, N, S, and O in the samples. The element distribution of NSCD comprised 29.16% C, 4.58% H, 21.69% N, 20.92% S, and 23.35% O, which were relatively equivalent to precursors. Meanwhile, the weight percentages in 5%-NSCD@MoS_2/G were calculated to be 9.22% C, 0.21% H, 0.19% N, 29.76% S, and 3.68% O. The decrease in the percentage of C, H, N, and O in the 5%-NSCD@MoS_2/G composite was attributed to the small proportion of NSCD in the composite and the loss of unattached NSCD on MoS_2/G nanosheets. The increase in S content might be due to the S content available in MoS_2.

The electrocatalytic HER activity of the NSCD@MoS_2/G composite, deposited on a glassy carbon electrode (GCE), was tested in 0.5 M H_2SO_4 using a three-electrode system (Supporting Information). The pure MoS_2 and pure G electrodes required onset potentials (at 1 mA cm^{-2}) of −127 and −418 mV vs RHE for the HER, respectively. Figure S6 displays that the pristine G obtained current density of 10 mA cm^{-2} at 500 mV. We determined the optimal MoS_2/G ratio for the HER activity by varying the weight ratios of MoS_2 and G at 0.75:1, 1:1, 1.25:1, 1.5:1, and 2:1. Figure 4a shows that the pristine MoS_2 obtained current density of 10 mA cm^{-2} at 231 mV. Among various mixed weight ratios, the combination of MoS_2 and G with a weight ratio of 1.25:1 (MoS_2/G, w/w) resulted in the highest HER activity with an onset potential of −51 mV and the overpotentials of 142 and 314 mV at 10 and 100 mA cm^{-2}, respectively. Figure 4b shows that the MoS_2/G (1.25:1, w/w) composite had a Tafel slope of 96 mV dec^{-1}. The enhanced HER performance of the binary composites, as compared to that of the pristine MoS_2, resulted from the integration of MoS_2 nanosheets and G nanosheets that established a van der Waals heterojunction force to reduce the barrier for the interfacial charge transfer of the binary composite.[10] Also, the plasma-induced ultrathin G nanosheets with high electrochemically active surface area and good conductivity facilitated the uniform distribution of MoS_2 nanosheets with numerous exposed sites, thereby promoting the proton adsorption and the release of H_2.

The effect of NSCD on the HER activity of ternary composites was investigated by mixing various concentrations of NSCD precursors to MoS_2/G (1.25:1) film to form ternary composites, including 2%-, 5%-, 7%-, and 10%-NSCD@MoS_2/G. Figure 4c reveals that the incorporation of 5 wt % NSCD into the ternary composite (5%-NSCD@MoS_2/G) gave the optimal HER performance with an overpotential value of 98 mV at a current density of 10 mA cm^{-2}. The remaining samples, including 2%-, 7%-, and 10%-NSCD@MoS_2/G composites delivered 105, 167, and 175 mV at 10 mA cm^{-2}, respectively. Remarkably, a less than 5% amount of NSCD incorporated into the MoS_2/G decreased the overpotential by 37 mV (from 142 to 105 mV) at 10 mA cm^{-2}. In contrast, a more than 5% amount of NSCD incorporated into the MoS_2/G; the HER performance degraded as the overpotentials increased by 25 and 33 mV at 10 mA cm^{-2} for 7 and 10% NSCD, respectively. Two driving forces can explain this phenomenon behind the performances: (i) interfacial interaction between the NSCD with MoS_2 and G; (ii) aggregation of NSCD. The NSCD had interfacial interactions with MoS_2 and G, which would facilitate their dispersion and intercalation in MoS_2 and G when a small amount of NSCD (2 and 5%) was present in the ternary composites, leading to an increase in the catalytic sites and their interfacial electron transfer for HER.[52] In contrast, the relatively larger amount of NSCD (7 and 10%) in the ternary composites would form aggregated multiple carbon layers that restricted the active sites of MoS_2 from proton adsorption, thus suppressing the HER efficiency. This trend is in good consistency with that of previous studies.[53,54] Furthermore, Figure 4d shows that the Tafel slope of the 5%-NSCD@MoS_2/G composite was the lowest (53 mV dec^{-1}) among the composites prepared at other ratios, indicating a desorption process in the Volmer−Heyrovsky reaction following the rate-determining step.[55] To evaluate the effect of N,S doping on the catalytic performance of NSCD@MoS_2/G, the electrochemical performance of pure carbon dot-anchored MoS_2/G (5%-CD@MoS_2/G) was tested. As displayed in Figure S7a,b, the overpotential and Tafel slope of the 5%-CD@MoS_2/G catalyst were 126 mV (at 10 mA cm^{-2}) and 65 mV Dec^{-1}, respectively. Compared to pure CD, the N,S-co-doped CD could decrease the overpotential of the composite to 28 mV. Substitutional N,S-doping into the carbon network can harmonize the chemical properties and increase active sites and electron distribution with a synergistic effect, resulting in significant enhancement of the catalytic activity of carbon dots. It has been reported that co-doping by two or three elements can significantly enhance the activity of pyridinic N through a dopant−carbon bridge, resulting in synergistic coupling between the dopants.[56]

In summary, the suitable incorporated amount of NSCD (5 wt %) could decrease the overpotential and Tafel slope of the MoS_2/G (1.25:1) composite by 44 mV (at 10 mA cm^{-2}) and 43 mV dec^{-1}, respectively. We attribute the excellent HER performance of the 5%-NSCD@MoS_2/G electrocatalyst to strong electrochemical coupling among the NSCD, MoS_2 nanosheets, and G nanosheets. First, chemical coupling facilitated the intercalation of highly dispersed NSCD of small size (<5 nm) to the MoS_2/G composite, further modifying electronic structure. Second, the outstanding charge transfer properties of the NSCD allowed it to accelerate electron transport from MoS_2 and G nanosheets to the GCE in an interconnected conducting network. Third, the N,S co-doping could enhance the intramolecular charge transfer of

https://doi.org/10.1021/acsaem.2c02401
ACS Appl. Energy Mater. 2022, 5, 12817−12827

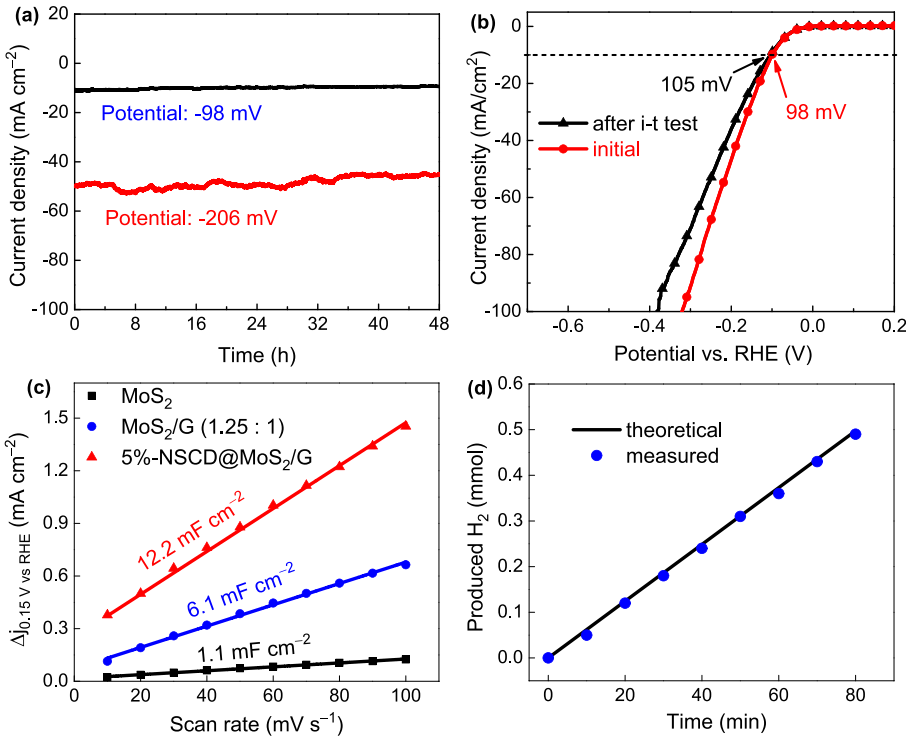

Figure 5. (a) Stability (i−t testing) test of the 5%-NSCD@MoS_2/G ternary composite measured at constant overpotentials of 98 and 206 mV for current densities of 10 and 50 mA cm^{-2}, respectively. (b) Polarization curves of the 5%-NSCD@MoS_2/G composite were recorded before and after a 48 h stability test. (c) Capacitive currents of MoS_2, MoS_2/G (1.25:1 w/w), and 5%-NSCD@MoS_2/G, plotted with respect to the scan rate. (d) Experimental and theoretical amounts of H_2 produced by the 5%-NSCD@MoS_2/G electrode at a fixed current density of 20 mA cm^{-2}.

NSCD to capture H^+ in the solution to form protonated groups and then transfer to MoS_2 to turn into H_2 gas.[57] As a result, the NSCD served as the critical factor in boosting the HER activity of the NSCD@MoS_2/G composite by enhancing both the number of active edge sites and the electron transport.

Furthermore, we used electrochemical impedance spectroscopy (EIS) to investigate the electrode kinetics, revealing evidence for the HER activity of the NSCD@MoS_2 composite. We set the frequency in the range from 0.1 Hz to 100 kHz to investigate the HER processes of our materials. By fitting the impedance data using a Randle electrical equivalent circuit, we obtained a model incorporating the solution resistance (R_s or R_1), charge transfer resistance (R_{CT} or R_2), constant phase element (CPE), and diffusion of ions in electrolyte solution represented by the Warburg region (W_{s1}). The values of R_s were in the range of 10−15 Ω with obvious semicircles for all cases. Figure 4e reveals that the lowest value of R_{CT} occurred when the MoS_2/G ratio was 1.25:1 (79 Ω). The addition of a suitable amount of G enhanced the electron transport of MoS_2, leading to a lower value of R_{CT}, presumably because the G nanosheets exhibited good adhesion and electrical contact with the substrate. Subsequently, the conductivity of the MoS_2/G composite was continuously increased in the presence of NSCD. The value of R_{CT} was lowest (Figure 4f) for the 5%-NSCD@MoS_2/G composite (47 Ω), which means that the electrical conductivity of this material was the highest among the composites prepared with different NSCD doping percentages. In comparison, 5%-pure-CD@MoS_2/G had an R_{CT} value of 180 Ω, as shown in Figure S7c, demonstrating the effect of N,S doping the on carbon framework. The co-doped N,S with different electronegativities combined into a hexagonal ring could act as the Lewis basic sites, which then donate p electrons to the π system, forming sp^2- and sp^3-hybridized bonds. As a result, it can effectively boost charge transfer of the composite.

It has been reported that the HER activity can be improved by decreasing the low contact resistance between MoS_2 and glassy carbon electrode (GCE).[58] The incorporation of 5%-NSCD into the MoS_2/G nanosheets resulted in the lowest resistivity of the ternary composite, indicating that optimal amount of NSCD diminished the resistance of the MoS_2, thus enhancing the contact conductivity between the as-prepared material and the GCE.

We investigated the intrinsic electrocatalytic efficiency of Mo by calculating the turnover frequencies (TOFs) based on eq S1 (SI). The resultant TOFs for the 2%-, 5%-, 7%-, and 10%-NSCD@MoS_2/G composites were 0.19, 0.22, 0.20, and 0.18 s^{-1}, respectively, implying that the most extensive enhancement in the intrinsic HER activity occurred for the 5%-NSCD@MoS_2/G composite. These effects agree well with our EIS measurements, where the impedance of the 5%-NSCD@MoS_2/G composite was the lowest among the composites.

High durability plays a significant role in the possibility of the practical application of any electrocatalyst. The chronopotentiometry result signified that the NSCD@MoS_2/G ternary nanocomposite provided a stable HER activity in 0.5 M H_2SO_4. Figure 5a displays the stability of controlled potential electrolysis using the 5%-NSCD@MoS_2/G electrode when held at overpotentials of 98 and 206 mV for 48 h. No significant change in electrode performance occurred, with the current densities remaining relatively constant at approximately 10 mA cm^{-2} for 48 h. Variations were apparent, however, throughout the measurements at 50 mA cm^{-2}. Such variation

https://doi.org/10.1021/acsaem.2c02401
ACS Appl. Energy Mater. 2022, 5, 12817−12827

is due to the dynamic process of long-time stability that may be affected by various factors. For example, more bubbles released at higher overpotentials, as we observed visually at the electrode surface (Figure S8 and Video S2 in the Supporting Information). We attribute this long-term stability of the catalyst to the NSCD that can interact well with MoS_2 and G nanosheets to form relatively stable ternary composites. In addition, the steady carbon structure could effectively protect the composite from corrosion and aggregation. Moreover, Figure 5b reveals that the overpotential of the linear sweep voltammetry (LSV) curve at 10 mA cm^{-2} for the 5%-NSCD@MoS_2/G composite increased slightly, from 98 to 105 mV (by 7 mV), after 48 h. The high stability of the HER activity of our nanocomposite catalyst makes it a promising material for large-scale commercial applications. In addition, we characterized the composition of the NSCD@MoS_2/G composite after performing the stability test. Figure S9 reveals that the deconvolution of the Mo 3d, N 1s, O 1s, and S 2p XPS spectra after 48 h of HER stability testing was almost identical to that of the pristine composite. Nevertheless, the O 1s peaks had red-shifted relative to the original sample, suggesting a degree of oxidation of Mo and the formation of MoO_2. The negligible change in the composition of the NSCD@MoS_2/G composite signifies its high durability.

The possible catalytic mechanism of such extraordinary catalysts was elucidated by determining the double-layer capacitance (C_{dl}), which is proportional to the electrochemically active surface area (ECSA) of a catalyst, of the MoS_2, MoS_2/G (1.25:1), and 5%-NSCD@MoS_2/G electrodes in the range of 0−0.1 V (*vs* NHE) (Figure S10). We plotted the capacitive currents (Δj, mean of j_a and j_c) measured at 0.15 V against various scan rates from 10 to 100 mV s^{-1}. Figure 5c reveals that the value of C_{dl} derived from the slope of linearity for the 5%-NSCD@MoS_2/G composite (12.2 mF cm^{-2}) was nearly double that of the MoS_2/G composite (6.1 mF cm^{-2}) and 12 times that of pristine MoS_2 (1.1 mF cm^{-2}). The larger value of C_{dl} for the 5%-NSCD@MoS_2/G ternary composite, relative to that of the MoS_2/G binary composite, indicates that it had greater available surface-active sites, thereby enhancing the absorption of water molecules and ensuring close contact with the electrolyte, together improving the HER performance.

Moreover, we used gas chromatography (GC) to quantify the amount of H_2 produced during the HER activity over the 5%-NSCD@MoS_2/G electrocatalyst at a fixed current density of 20 mA cm^{-2} within 80 min to investigate the Faradic efficiency. Figure 5d reveals the high stability of the catalyst, as evidenced by the constant rate of H_2 production during the HER experiment; it was almost the same as the theoretically calculated H_2 production yield (eq S2, SI), suggesting a Faradaic efficiency of close to 100%. After 80 min of reaction, the amount of H_2 produced was calculated to be 490 μmol. We attribute the outstanding HER performance of the NSCD@MoS_2/G ternary composite to the presence of the NSCD, which incorporated almost homogeneously into the MoS_2/G binary composite, thereby ensuring intimate contact between the catalyst and the electrolyte and propitious to gas release through water splitting. In addition, the NSCD was intercalated in a few layers of MoS_2 and G nanosheets, thereby providing plentiful exposed edges and an abundance of active sites for catalytic HER reactions. Furthermore, the NSCD enhanced electron transfer from the inner to the outer layer of the MoS_2/G binary composite. Table S3 compares the HER performance of our NSCD@MoS_2/G composite with those of other HER electrocatalysts reported previously. Based on this benchmark table, we conclude that our ternary composite can be synthesized within a shorter time and give better HER activity than most catalysts based on non-noble metals.

■ CONCLUSIONS

We have used a facile surface-plasma-induced approach performed at low temperature (60 °C) in a short time (45 min) for fabricating a stable NSCD@MoS_2/G ternary composite electrocatalyst that possesses highly efficient HER activity. This approach enabled us to intercalate NSCD into the MoS_2/G binary composites and tune their interlayer structures, improving the conductivity and increasing the number of active sites, thereby enhancing the HER catalytic performance. Compared to pristine MoS_2, pristine G, and MoS_2/G binary composites, the as-synthesized NSCD@MoS_2/G ternary composite exhibited its superior HER activity with low onset potential (−37 mV at 1 mA cm^{-2}), small overpotential (98 mV at 10 mA cm^2), low Tafel slope (53 mV dec^{-1}), and excellent durability (48 h i-t testing). We attribute the excellent HER performance of NSCD@MoS_2/G to two reasons. First, the loading matrix with ultrathin G nanosheets can generate more atom edge active sites and defects, resulting in the enhanced conductivity of MoS_2. Second, the synergistic manipulation of NSCD tunes the electron density by interacting at the interface of MoS_2 and G, accelerating electron transport from the composite to GCE. Therefore, this study not only utilized a facile and rapid method for synthesizing 2D material-based composites doped with carbon dots but also provided a mechanism for optimizing the performance of large-scale HER catalysts.

■ ASSOCIATED CONTENT

Supporting Information

The Supporting Information is available free of charge at https://pubs.acs.org/doi/10.1021/acsaem.2c02401.

Experimental details including chemicals and the ratios of components for synthesizing composites, theoretical calculations for TOF and hydrogen gas production, comparison of the synthetic methods and HER performance of recently reported Mo- and carbon dot-based materials, and additional data including SEM, TEM, XRD pattern, Raman shift, size distribution, XPS, and electrochemical characterization (PDF)

Plasma exfoliation (MP4)

Hydrogen production (MP4)

■ AUTHOR INFORMATION

Corresponding Author

Kung-Hwa Wei − *Department of Materials Science and Engineering and Center for Emergent Functional Matter Science, National Yang Ming Chiao Tung University, Hsinchu 30010, Taiwan;* orcid.org/0000-0002-0248-4091; Email: khwei@nycu.edu.tw

Authors

Van Dien Dang − *Department of Materials Science and Engineering, National Yang Ming Chiao Tung University, Hsinchu 30010, Taiwan; Faculty of Biology and Environment, Ho Chi Minh University of Food Industry, Ho Chi Minh 700000, Vietnam;* orcid.org/0000-0003-0864-7389

https://doi.org/10.1021/acsaem.2c02401
ACS Appl. Energy Mater. 2022, 5, 12817−12827

Chang-Yu Hsiao − *Department of Materials Science and Engineering, National Yang Ming Chiao Tung University, Hsinchu 30010, Taiwan*
Phuoc Anh Le − *Faculty of Textile Science and Technology, Shinshu University, Nagano 386-0018, Japan; Institute of Sustainability Science, Vietnam-Japan University, Vietnam National University-Hanoi, Hanoi 100000, Vietnam*
Van Qui Le − *Department of Materials Science and Engineering, National Yang Ming Chiao Tung University, Hsinchu 30010, Taiwan*
Dang Ho Phuong Thao − *Faculty of Biology and Environment, Ho Chi Minh University of Food Industry, Ho Chi Minh 700000, Vietnam*
Thi-Hien Do − *Department of Materials Science and Engineering, National Yang Ming Chiao Tung University, Hsinchu 30010, Taiwan*

Complete contact information is available at:
https://pubs.acs.org/10.1021/acsaem.2c02401

Notes

The authors declare no competing financial interest.

■ ACKNOWLEDGMENTS

This study was performed under the auspices of National Science and Technology Council, Taiwan (grant nos.: NSTC 109-2221-E-009-064-MY3 and NSTC 110-2221-E-A49-046-MY3, NSTC 111-2634-F-A49-007) and the Center for Emergent Functional Matter Science of National Yang Ming Chiao Tung University from The Featured Areas Research Center Program within the framework of the Higher Education Sprout Project by the Ministry of Education (MOE) in Taiwan.

■ REFERENCES

(1) Lu, A.-Y.; Zhu, H.; Xiao, J.; Chuu, C.-P.; Han, Y.; Chiu, M.-H.; Cheng, C.-C.; Yang, C.-W.; Wei, K.-H.; Yang, Y.; Wang, Y.; Sokaras, D.; Nordlund, D.; Yang, P.; Muller, D. A.; Chou, M. Y.; Zhang, X.; Li, L. J. Janus Monolayers of Transition Metal Dichalcogenides. *Nat. Nanotechnol.* **2017**, *12*, 744−749.
(2) Sajedi-Moghaddam, A.; Saievar-Iranizad, E.; Pumera, M. Two-Dimensional Transition Metal Dichalcogenide/Conducting Polymer Composites: Synthesis and Applications. *Nanoscale* **2017**, *9*, 8052−8065.
(3) Bar-Ziv, R.; Ranjan, P.; Lavie, A.; Jain, A.; Garai, S.; Bar Hen, A.; Popovitz-Biro, R.; Tenne, R.; Arenal, R.; Ramasubramaniam, A.; Lajaunie, L.; Bar-Sadan, M. Au-MoS_2 Hybrids as Hydrogen Evolution Electrocatalysts. *ACS Appl. Energy Mater.* **2019**, *2*, 6043−6050.
(4) Nguyen, V.-T.; Le, P. A.; Hsu, Y.-C.; Wei, K.-H. Plasma-Induced Exfoliation Provides Onion-Like Graphene-Surrounded MoS_2 Nanosheets for a Highly Efficient Hydrogen Evolution Reaction. *ACS Appl. Mater. Interfaces* **2020**, *12*, 11533−11542.
(5) Najafi, L.; Bellani, S.; Oropesa-Nuñez, R.; Ansaldo, A.; Prato, M.; Del Rio Castillo, A. E.; Bonaccorso, F. Engineered $MoSe_2$-Based Heterostructures for Efficient Electrochemical Hydrogen Evolution Reaction. *Adv. Energy Mater.* **2018**, *8*, 1703212.
(6) Zhang, L.-N.; Li, S.-H.; Tan, H.-Q.; Khan, S. U.; Ma, Y.-Y.; Zang, H.-Y.; Wang, Y.-H.; Li, Y.-G. MoP/Mo_2C@C: A New Combination of Electrocatalysts for Highly Efficient Hydrogen Evolution over the Entire pH Range. *ACS Appl. Mater. Interfaces* **2017**, *9*, 16270−16279.
(7) Jiao, Y.; Yan, H.; Wang, R.; Wang, X.; Zhang, X.; Wu, A.; Tian, C.; Jiang, B.; Fu, H. Porous Plate-like MoP Assembly as an Efficient pH-Universal Hydrogen Evolution Electrocatalyst. *ACS Appl. Mater. Interfaces* **2020**, *12*, 49596−49606.
(8) Iffelsberger, C.; Pumera, M. High Resolution Electrochemical Additive Manufacturing of Microstructured Active Materials: Case Study of MoS_x as a Catalyst for the Hydrogen Evolution Reaction. *J. Mater. Chem. A* **2021**, *9*, 22072−22081.
(9) Hinnemann, B.; Moses, P. G.; Bonde, J.; Jørgensen, K. P.; Nielsen, J. H.; Horch, S.; Chorkendorff, I.; Nørskov, J. K. Biomimetic Hydrogen Evolution: MoS_2 Nanoparticles as Catalyst for Hydrogen Evolution. *J. Am. Chem. Soc.* **2005**, *127*, 5308−5309.
(10) Gnanasekar, P.; Periyanagounder, D.; Kulandaivel, J. Vertically Aligned MoS_2 Nanosheets on Graphene for Highly Stable Electrocatalytic Hydrogen Evolution Reactions. *Nanoscale* **2019**, *11*, 2439−2446.
(11) Anjum, M. A. R.; Jeong, H. Y.; Lee, M. H.; Shin, H. S.; Lee, J. S. Efficient Hydrogen Evolution Reaction Catalysis in Alkaline Media by All-In-One MoS_2 with Multifunctional Active Sites. *Adv. Mater.* **2018**, *30*, 1707105.
(12) Chen, J.; Liu, G.; Zhu, Y. Z.; Su, M.; Yin, P.; Wu, X. J.; Lu, Q.; Tan, C.; Zhao, M.; Liu, Z.; Yang, W.; Li, H.; Nam, G. H.; Zhang, L.; Chen, Z.; Huang, X.; Radjenovic, P. M.; Huang, W.; Tian, Z. Q.; Li, J. F.; Zhang, H. Ag@MoS_2 Core−Shell Heterostructure as SERS Platform to Reveal the Hydrogen Evolution Active Sites of Single-Layer MoS_2. *J. Am. Chem. Soc.* **2020**, *142*, 7161−7167.
(13) Debbarma, R.; Nguyen, N. H. L.; Berry, V. Defect Guided Conduction in Graphene-Derivatives and MoS_2: Two-Dimensional Nanomaterial Models. *Appl. Mater. Today* **2021**, *23*, 101072.
(14) Mazánek, V.; Luxa, J.; Matějková, S.; Kučera, J.; Sedmidubský, D.; Pumera, M.; Sofer, Z. Ultrapure Graphene Is a Poor Electrocatalyst: Definitive Proof of the Key Role of Metallic Impurities in Graphene-Based Electrocatalysis. *ACS Nano* **2019**, *13*, 1574−1582.
(15) Pumera, M. Materials Electrochemists' Never-Ending Quest for Efficient Electrocatalysts: The Devil Is in the Impurities. *ACS Catal.* **2020**, *10*, 7087−7092.
(16) Jaramillo, T. F.; Jørgensen, K. P.; Bonde, J.; Nielsen, J. H.; Horch, S.; Chorkendorff, I. Identification of Active Edge Sites for Electrochemical H_2 Evolution from MoS_2 Nanocatalysts. *Science* **2007**, *317*, 100−102.
(17) Wang, X.; Fei, Y.; Wang, W.; Yuan, W.; Li, C. M. Polymer-Mediated Self-Assembly of Amorphous Metal−Organic Complexes toward Fabrication of Three-Dimensional Graphene Supported CoP Nanoparticle-Embedded N-Doped Carbon as a Superior Hydrogen Evolution Catalyst. *ACS Appl. Energy Mater.* **2019**, *2*, 8851−8861.
(18) Holá, K.; Pavliuk, M. V.; Németh, B.; Huang, P.; Zdražil, L. S.; Land, H.; Berggren, G.; Tian, H. Carbon Dots and [FeFe] Hydrogenase Biohybrid Assemblies for Efficient Light-Driven Hydrogen Evolution. *ACS Catal.* **2020**, *10*, 9943−9952.
(19) Liu, Y.; Li, X.; Zhang, Q.; Li, W.; Xie, Y.; Liu, H.; Shang, L.; Liu, Z.; Chen, Z.; Gu, L.; Tang, Z.; Zhang, T.; Lu, S. A General Route to Prepare Low-Ruthenium-Content Bimetallic Electrocatalysts for pH-Universal Hydrogen Evolution Reaction by Using Carbon Quantum Dots. *Angew. Chem., Int. Ed.* **2020**, *59*, 1718−1726.
(20) Wu, H.; Lu, S.; Yang, B. Carbon-Dot-Enhanced Electrocatalytic Hydrogen Evolution. *Acc. Mater. Res.* **2022**, *3*, 319−330.
(21) Dang, Q.; Sun, Y.; Wang, X.; Zhu, W.; Chen, Y.; Liao, F.; Huang, H.; Shao, M. Carbon Dots-Pt Modified Polyaniline Nanosheet Grown on Carbon Cloth as Stable and High-Efficient Electrocatalyst for Hydrogen Evolution in pH-Universal Electrolyte. *Appl. Catal., B* **2019**, *257*, 117905.
(22) Jin, L.; Zhao, H.; Wang, Z. M.; Rosei, F. Quantum Dots-Based Photoelectrochemical Hydrogen Evolution from Water Splitting. *Adv. Energy Mater.* **2021**, *11*, 2003233.
(23) Song, H.; Yu, J.; Tang, Z.; Yang, B.; Lu, S. Halogen-Doped Carbon Dots on Amorphous Cobalt Phosphide as Robust Electrocatalysts for Overall Water Splitting. *Adv. Energy Mater.* **2022**, *12*, 2102573.
(24) Su, C.-Y.; Lu, A.-Y.; Xu, Y.; Chen, F.-R.; Khlobystov, A. N.; Li, L.-J. High-Quality Thin Graphene Films from Fast Electrochemical Exfoliation. *ACS Nano* **2011**, *5*, 2332−2339.
(25) Coleman, J. N.; Lotya, M.; O'Neill, A.; Bergin, S. D.; King, P. J.; Khan, U.; Young, K.; Gaucher, A.; De, S.; Smith, R. J. Two-Dimensional Nanosheets Produced by Liquid Exfoliation of Layered Materials. *Science* **2011**, *331*, 568−571.

(26) Le, P.-A.; Nguyen, V. T.; Le, V. Q.; Lu, Y.-C.; Huang, S.-Y.; Sahoo, S. K.; Chu, Y.-H.; Wei, K.-H. One-Step Surface-Plasma-Induced Exfoliation of the Graphite/WS_2 Bilayer into Homogeneous Two-Dimensional Graphene/WS_2 Nanosheet Composites as Catalysts for the Hydrogen Evolution Reaction. *ACS Appl. Energy Mater.* **2021**, *4*, 5143−5154.
(27) Sun, X.; Dai, J.; Guo, Y.; Wu, C.; Hu, F.; Zhao, J.; Zeng, X.; Xie, Y. Semimetallic Molybdenum Disulfide Ultrathin Nanosheets as an Efficient Electrocatalyst for Hydrogen Evolution. *Nanoscale* **2014**, *6*, 8359−8367.
(28) Ali, B. A.; Omar, A. M. A.; Khalil, A. S. G.; Allam, N. K. Untapped Potential of Polymorph MoS_2: Tuned Cationic Intercalation for High-Performance Symmetric Supercapacitors. *ACS Appl. Mater. Interfaces* **2019**, *11*, 33955−33965.
(29) Geng, J.; Kong, B.-S.; Yang, S. B.; Jung, H.-T. Preparation of Graphene Relying on Porphyrin Exfoliation Of Graphite. *Chem. Commun.* **2010**, *46*, 5091−5093.
(30) Lu, X.; Utama, M. I. B.; Lin, J.; Luo, X.; Zhao, Y.; Zhang, J.; Pantelides, S. T.; Zhou, W.; Quek, S. Y.; Xiong, Q. Rapid and Nondestructive Identification of Polytypism and Stacking Sequences in Few-Layer Molybdenum Diselenide by Raman Spectroscopy. *Adv. Mater.* **2015**, *27*, 4502−4508.
(31) Coy Diaz, H.; Addou, R.; Batzill, M. Interface properties of CVD grown graphene transferred onto MoS_2 (0001). *Nanoscale* **2014**, *6*, 1071−1078.
(32) Huang, S.-Y.; Le, P.-A.; Nguyen, V.-T.; Lu, Y.-C.; Sung, C.-W.; Cheng, H.-W.; Hsiao, C.-Y.; Dang, V. D.; Chiu, P.-W.; Wei, K.-H. Surface Plasma−Induced Tunable Nitrogen Doping Through Precursors Provides 1T-2H $MoSe_2$/Graphene Sheet Composites as Electrocatalysts for the Hydrogen Evolution Reaction. *Electrochim. Acta* **2022**, *426*, 140767.
(33) Ramakrishna Matte, H.; Gomathi, A.; Manna, A. K.; Late, D. J.; Datta, R.; Pati, S. K.; Rao, C. MoS_2 and WS_2 Analogues of Graphene. *Angew. Chem., Int. Ed.* **2010**, *49*, 4059−4062.
(34) Sun, D.; Huang, D.; Wang, H.; Xu, G.-L.; Zhang, X.; Zhang, R.; Tang, Y.; Abd Ei-Hady, D.; Alshitari, W.; Saad Al-Bogami, A.; Amine, K.; Shao, M. 1T MoS_2 Nanosheets with Extraordinary Sodium Storage Properties via Thermal-Driven Ion Intercalation Assisted Exfoliation of Bulky MoS_2. *Nano Energy* **2019**, *61*, 361−369.
(35) Sandoval, S. J.; Yang, D.; Frindt, R.; Irwin, J. Raman Study and Lattice Dynamics of Single Molecular Layers of MoS_2. *Phys. Rev. B* **1991**, *44*, 3955.
(36) Nardekar, S. S.; Krishnamoorthy, K.; Pazhamalai, P.; Sahoo, S.; Mariappan, V. K.; Kim, S.-J. Exceptional Interfacial Electrochemistry of Few-Layered 2D MoS_2 Quantum Sheets for High Performance Flexible Solid-State Supercapacitors. *J. Mater. Chem. A* **2020**, *8*, 13121−13131.
(37) Pollard, A. J.; Brennan, B.; Stec, H.; Tyler, B. J.; Seah, M. P.; Gilmore, I. S.; Roy, D. Quantitative Characterization of Defect Size in Graphene Using Raman Spectroscopy. *Appl. Phys. Lett.* **2014**, *105*, 253107.
(38) Reckmeier, C. J.; Schneider, J.; Susha, A. S.; Rogach, A. L. Luminescent Colloidal Carbon Dots: Optical Properties and Effects of Doping. *Opt. Express* **2016**, *24*, A312−A340.
(39) Dang, V. D.; Adorna, J.; Annadurai, T.; Bui, T. A. N.; Tran, H. L.; Lin, L.-Y.; Doong, R.-A. Indirect Z-scheme Nitrogen-Doped Carbon Dot Decorated Bi_2MoO_6/g-C_3N_4 Photocatalyst for Enhanced Visible-Light-Driven Degradation of Ciprofloxacin. *Chem. Eng. J.* **2021**, *422*, 130103.
(40) Luo, J.; Zhou, Y.; Tuo, Y.; Gu, Y.; Wang, X.; Guo, Q.; Chen, C.; Wang, D.; Wang, S.; Zhang, J. Interfacial Polarization in Ultra-Small Co_3S_4−MoS_2 Heterostructure for Efficient Electrocatalytic Hydrogen Evolution Reaction. *Appl. Mater. Today* **2022**, *26*, 101311.
(41) Chang, K.; Hai, X.; Pang, H.; Zhang, H.; Shi, L.; Liu, G.; Liu, H.; Zhao, G.; Li, M.; Ye, J. Targeted Synthesis of 2H- and 1T-phase MoS_2 Monolayers for Catalytic Hydrogen Evolution. *Adv. Mater.* **2016**, *28*, 10033−10041.
(42) He, X.; Yin, F.; Chen, B.; Li, G.; Yin, H. "Bulk" 1T/2H-MoS_2 with Tunable Phases and Residual S, N Co-Doped Carbon as a Highly Active and Durable Catalyst for Hydrogen Evolution. *ACS Appl. Energy Mater.* **2019**, *2*, 2022−2033.
(43) Lu, A.-Y.; Yang, X.; Tseng, C.-C.; Min, S.; Lin, S.-H.; Hsu, C.-L.; Li, H.; Idriss, H.; Kuo, J.-L.; Huang, K.-W.; Li, L.-J. High-Sulfur-Vacancy Amorphous Molybdenum Sulfide as a High Current Electrocatalyst in Hydrogen Evolution. *Small* **2016**, *12*, 5530−5537.
(44) Liu, Q.; Li, X.; He, Q.; Khalil, A.; Liu, D.; Xiang, T.; Wu, X.; Song, L. Gram-Scale Aqueous Synthesis of Stable Few-Layered 1T-MoS_2: Applications for Visible-Light-Driven Photocatalytic Hydrogen Evolution. *Small* **2015**, *11*, 5556−5564.
(45) Baker, M. A.; Gilmore, R.; Lenardi, C.; Gissler, W. XPS Investigation of Preferential Sputtering of S from MoS_2 and Determination of MoS_x Stoichiometry from Mo and S Peak Positions. *Appl. Surf. Sci.* **1999**, *150*, 255−262.
(46) Lukowski, M. A.; Daniel, A. S.; Meng, F.; Forticaux, A.; Li, L.; Jin, S. Enhanced Hydrogen Evolution Catalysis from Chemically Exfoliated Metallic MoS_2 Nanosheets. *J. Am. Chem. Soc.* **2013**, *135*, 10274−10277.
(47) Bhunia, S. K.; Jana, N. R. Reduced Graphene Oxide-Silver Nanoparticle Composite as Visible Light Photocatalyst for Degradation of Colorless Endocrine Disruptors. *ACS Appl. Mater. Interfaces* **2014**, *6*, 20085−20092.
(48) Zhang, J.; Yuan, Y.; Gao, M.; Han, Z.; Chu, C.; Li, Y.; van Zijl, P. C. M.; Ying, M.; Bulte, J. W. M.; Liu, G. Carbon Dots as a New Class Of Diamagnetic Chemical Exchange Saturation Transfer (DiaCEST) MRI Contrast Agents. *Angew. Chem., Int. Ed.* **2019**, *58*, 9871−9875.
(49) Park, S.-W.; Jang, B.; Kim, H.; Lee, J.; Park, J. Y.; Kang, S.-O.; Choa, Y.-H. Highly Water-Dispersible Graphene Nanosheets from Electrochemical Exfoliation of Graphite. *Front. Chem.* **2021**, *9*, 519.
(50) Zhou, G.; Wang, D.-W.; Yin, L.-C.; Li, N.; Li, F.; Cheng, H.-M. Oxygen Bridges between NiO Nanosheets and Graphene for Improvement of Lithium Storage. *ACS Nano* **2012**, *6*, 3214−3223.
(51) Liu, X.; Amiinu, I. S.; Liu, S.; Pu, Z.; Li, W.; Ye, B.; Tan, D.; Mu, S. H_2O_2-Assisted Synthesis of Porous N-Doped Graphene/Molybdenum Nitride Composites with Boosted Oxygen Reduction Reaction. *Adv. Mater. Interfaces* **2017**, *4*, 1601227.
(52) Pei, X.; Xiong, D.; Wang, H.; Gao, S.; Zhang, X.; Zhang, S.; Wang, J. Reversible Phase Transfer of Carbon Dots between an Organic Phase and Aqueous Solution Triggered by CO_2. *Am. Ethnol.* **2018**, *130*, 3749−3753.
(53) Liu, Y.; Yang, Y.; Peng, Z.; Liu, Z.; Chen, Z.; Shang, L.; Lu, S.; Zhang, T. Self-Crosslinking Carbon Dots Loaded Ruthenium Dots as an Efficient and Super-Stable Hydrogen Production Electrocatalyst at all pH Values. *Nano Energy* **2019**, *65*, 104023.
(54) Wang, L.; Wu, X.; Guo, S.; Han, M.; Zhou, Y.; Sun, Y.; Huang, H.; Liu, Y.; Kang, Z. Mesoporous Nitrogen, Sulfur Co-Doped Carbon Dots/CoS Hybrid as an Efficient Electrocatalyst for Hydrogen Evolution. *J. Mater. Chem. A* **2017**, *5*, 2717−2723.
(55) Li, Y.; Wang, H.; Xie, L.; Liang, Y.; Hong, G.; Dai, H. MoS_2 Nanoparticles Grown on Graphene: An Advanced Catalyst for the Hydrogen Evolution Reaction. *J. Am. Chem. Soc.* **2011**, *133*, 7296−7299.
(56) Duan, X.; O'Donnell, K.; Sun, H.; Wang, Y.; Wang, S. Sulfur and Nitrogen Co-Doped Graphene for Metal-Free Catalytic Oxidation Reactions. *Small* **2015**, *11*, 3036−3044.
(57) Li, W.; Liu, Y.; Wu, M.; Feng, X.; Redfern, S. A. T.; Shang, Y.; Yong, X.; Feng, T.; Wu, K.; Liu, Z.; Li, B.; Chen, Z.; Tse, J. S.; Lu, S.; Yang, B. Carbon-Quantum-Dots-Loaded Ruthenium Nanoparticles as an Efficient Electrocatalyst for Hydrogen Production in Alkaline Media. *Adv. Mater.* **2018**, *30*, 1800676.
(58) Voiry, D.; Fullon, R.; Yang, J.; de Carvalho Castro e Silva, C.; Kappera, R.; Bozkurt, I.; Kaplan, D.; Lagos, M. J.; Batson, P. E.; Gupta, G. The Role of Electronic Coupling between Substrate and 2D MoS_2 Nanosheets in Electrocatalytic Production of Hydrogen. *Nat. Mater.* **2016**, *15*, 1003−1009.

https://doi.org/10.1021/acsaem.2c02401
ACS Appl. Energy Mater. 2022, 5, 12817−12827